Proceedings of the Pakistan Academy of Sciences: A: Physical and Computational Sciences 58(4): 17-26 (2021)

ISSN (Print): 2518-4245; ISSN (Online): 2518-4253
https://doi.org/10.53560/PPASA(58-4)759

Pakistan Academy of Sciences

Research Article

Fractional Order Neural Transient Modeling of Primary Circuit of ACP1000 Based Nuclear Power Plant in LabVIEW

Arshad H. Malik[1*], Aftab A. Memon[2], and Feroza Arshad[3]

[1]Department of Maintenance Training, Pakistan Atomic Energy Commission, A-104, Block-B, Kazimablad, Model Colony, Karachi, Pakistan
[2]Department of Telecommunication Engineering, Mehran University of Engineering and Technology, Jamshoro, Sindh, Pakistan
[3]Department of Management Information System, Pakistan Atomic Energy Commission, B-63, Block-B, Kazimablad, Model Colony, Karachi, Pakistan

Abstract: The primary circuit of the nuclear power plant is the most advanced and sophisticated loop of the Advanced Chinese Pressurized Water Reactor (ACP1000). The primary circuit is composed of most technologically advanced nuclear systems and controllers. In this research work, closed loop dynamics of primary circuit (CLPC) of ACP1000 based nuclear power plant is identified. The closed loop dynamics is comprised of highly nonlinear coupled seven control systems. The turbine power, pressurizer temperature, cold leg temperature, hot leg temperature, coolant average temperature and feed water flow are the selected parameters of interest as inputs while neutron power, reactor coolant pressure, pressurizer level, steam generator pressure, steam generator level and steam generator flow as outputs. Therefore, a closed loop multi-input multi-out (MIMO) is configured. The control oriented closed loop dynamics of the primary circuit of ACP1000 is estimated by state-of-the-art novel fractional order neural network (FO-ANN) tool developed in LabVIEW. The parameters of FO-ANN of CLPC (FO-ANN-CLPC) are optimized using fractional order backpropagation (FO-BP) algorithm. The performance of FO-ANN-CLPC is tested and validated in transient conditions and the proposed model predicted the desired reactor power with minimizing error function. The robust performance of the proposed closed loop model is evaluated by dynamic simulation for a prescribed turbine load power increase transient from 20 % to 100 % and validated against reactor power and behaviour of various thermal hydraulics parameters are observed and analyzed.

Keywords: Fractional Order, Neural Estimation, Primary Circuit, Coupled Systems, ACP1000, Nuclear Power Plant, LabVIEW

1. INTRODUCTION

In this research work, the most advanced and most sophisticated third generation Advanced Chinese Pressurized Water Reactor of 1100 MWe (ACP1000) is taken into account for closed loop transient modeling of primary circuit of nuclear power plant [1-3].

A robust fractional order PID controller is designed for an uncertain research reactor [4]. Fractional order differential equations are solved and optimized by artificial neural networks in [5]. The dynamic analysis of fractional order recurrent neural network is performed in [6]. A research is further extended for variable order fractional delay differential equations optimized by neural error minimization technique. The parameters of artificial neural network are tuned by simulated annealing method [7]. Nonlinear dynamics identification is performed by neuro-fractional order Hammerstein model in [8]. Neuro-fractional order problems are solved via centralized and decentralized data sampling methods in a discrete domain [9]. Neural network based fractional order differential equations are solved for chaotic systems with

Received: August 2021; Accepted: December 2021
*Corresponding Author: Arshad H. Malik <mastermind_arshad@yahoo.com>

backlash nonlinearity [10]. A research is adopted for model reduction of large scale systems using fractional order neural networks [11]. A neural network is used to tackle the nonlinear fractional order systems for multi-model estimation and fault detection purposes [12]. A multilayer fractional order fault classifier is developed for X-rays image processing in LabVIEW [13]. A research is explored for stability analysis of fractional order neural time delay systems [14]. A wavelet neural network optimized fractional order PID controller is designed for Integrated PWR (IPWR) nuclear power plant load shedding studies [15]. The research is further extended to explore reactor power control in turbine load following scenarios for marine applications [16]. This type of study is very useful for PWR based nuclear power plants for load following purposes.

In this research work, a novel state-of-the-art coupled closed loop dynamic MIMO (CCLD-MIMO) model of primary circuit of ACP1000 is developed for the first time in LabVIEW incorporating nonlinear dynamics of reactor power control system (G-bank), reactor power control system (R-bank), pressurizer pressure control system, pressurizer level control system, digital electro-hydraulic control system, steam generator water level control system and steam dump control system. CCLD-MIMO model is structured in Fractional Order Back Propagation Artificial Neural Network (FO-BP-ANN) form in LabVIEW.

2. MATERIALS AND METHODS

2.1. Primary Circuit of ACP1000

The primary circuit of ACP1000 is comprised of systems responsible for reactor power generation in the reactor core in response to turbine load changes. The basic objective of this research work is to establish a relationship between reactor power and turbine power through various control systems associated with the primary loop of ACP1000 using the fractional order neural network technique. In order to account for the turbine load impact on the primary loop of ACP1000, the Digital Electro Hydraulic (DEH) control system is considered as a part of closed loop for dynamic analysis and simulation studies otherwise it is not needed to consider for modeling primary circuit. DEH is primarily a control system of secondary circuit but it is added to provide essential coupling between reactor power and turbine power.

2.2 Coupled Close Loop Dynamics of Primary Circuit Systems

There are seven control systems involved in the coupled dynamics of primary circuit of ACP1000. These seven controllers are reactor power control system (G-bank), reactor power control system (R-bank), pressurizer pressure control system, pressurizer level control system, digital electro-hydraulic control system, steam generator water level control system and steam dump control systems respectively. G-bank consists of sub G1-bank and sub G2-bank while R-bank is a single bank. G-bank has more worth than R-bank because it is meant for temperature control and reactor power control while R-bank is meant for power control only. The important key parameters are identified as inputs and outputs of closed loop control systems for precise dynamic estimations. The coupling of closed loop control systems and their associated input and output variables are shown in Figure 1.

2.3 Framework of FO-ANN-CLPC

Instead of designing the FO-ANN for each closed loop control system, the overall closed loop model

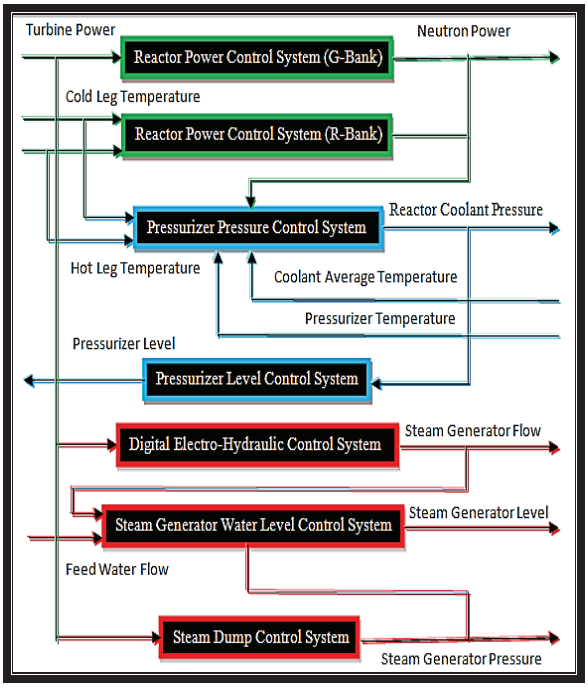

Fig. 1. Closed loop primary circuit of ACP1000.

is configured in MIMO form with six inputs and six outputs as shown in Figure 2.

The closed loop primary circuit of ACP1000 configured in MIMO form as shown in Fig. 1 is represented in symbolic form with detailed internal configuration in Figure 3.

2.4 FO-ANN Intelligent Learning

2.4.1 Idea of Fractional Order System

The fractional order dynamics is basically a system of differential equations containing non-integer order. The purpose of fractional order dynamics is to have improved complex signal processing, better control performance and enhanced optimization process with guaranteed convergence and finite behaviour.

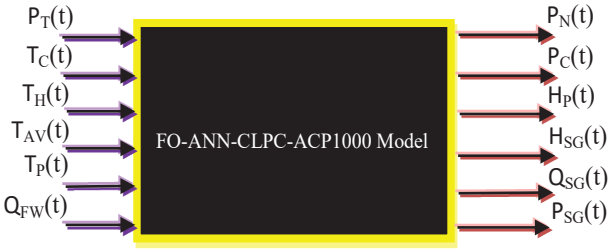

Fig. 2. FO-ANN-CLPC input-output MIMO configuration model of ACP1000.

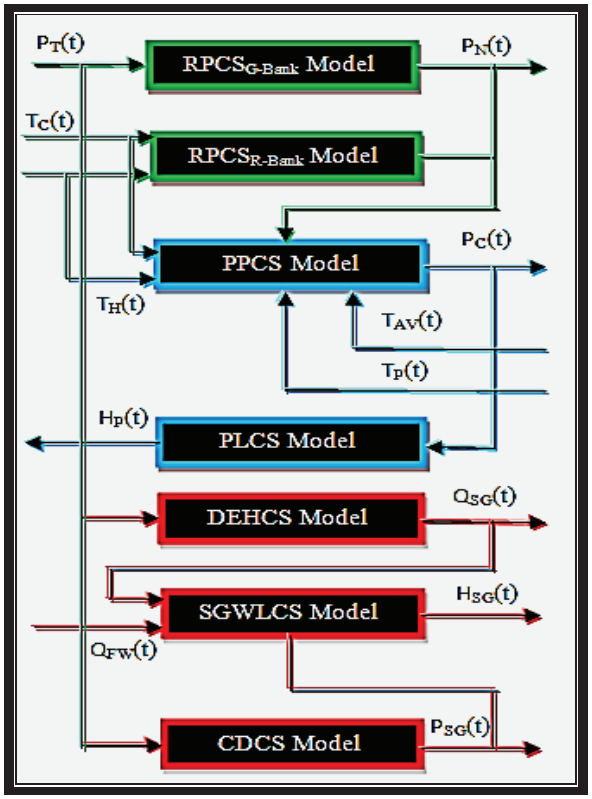

Fig. 3. Coupled symbolic internal architecture of FO-ANN-CLPC-ACP1000.

2.4.2 Choice of Machine Learning Algorithm

In this research work, fractional order machine learning is employed. The improved backpropagation algorithm is formulated in a fractional order fashion. This improved algorithm is formulated using Grunwald Letnikow fractional derivative approximation [8].

2.5 FO-ANN-CLPC-ACP1000 Modeling

2.5.1. Design Basis

Now, the input vector $u\ (i)$, $i = 1,2,3,..,6$ and output vector $y\ (j)$, $j = 1,2,3,..,6$ based on Fig. 2 are defined as: $u_i(k) = [P_T(k)\ T_C(k)\ T_H(k)\ T_{AV}(k)\ T_P(k)\ Q_{FW}(k)]^T$

$$y_j(k) = [P_N(k) P_C(k) H_P(k) H_{SG}(k) P_{SG}(k) Q_{SG}(k)]^T$$

Where k is the instant of discretization. The dimension of MIMO system is 6x6. If $p = i$ is the number of neurons or nodes in the input layer (n_p =1,2,3,….., p), q is the number of neurons in the hidden layer (nq =1,2,3,….., q) and $r = j$ is the number of neurons in the output layer (n_r =1,2,3,….., r) then W_I and W_H are the weight matrices of input and hidden layers comprised of $w_{np,nq}$ and $w_{nq,nr}$ weights respectively, B_I and B_H are bias vectors of input and hidden layers comprised of b_{nq} and b_{nr} bias elements respectively then $\theta_I(.)$ and $\theta_H(.)$ are nonlinear activation functions of input and hidden layers respectively.

2.5.2 Problem Formulation CCLD-MIMO Model

The basic idea presented by [8] is adopted to derive the formulation for CCLD-MIMO model of ACP1000.

Now, the error dynamics from input layer to hidden layer is calculated as:

$$e_{I\,n_q}(k) = \sum_{n_p=1}^{p} w_{np,nq} u_{n_p}(k) + b_{n_q} \tag{1}$$

The activation function associated with the hidden layer is given as:

$$\theta_{I\,n_q}(k) = f_I(e_{I\,n_q}(k)) \tag{2}$$

Now, the error dynamics from the input layer to output layer is calculated as:

$$e_{H n_r}(k) = \sum_{n_q=1}^{q} w_{nq,nr}\theta_{I n_q}(k) + b_{n_r}$$

The activation function associated with the hidden layer is given as:

$$\theta_{H n_r}(k) = f_H(e_{H_{n_r}}(k))$$

If α is fractional order of derivative function Dα, M is the discrete measurement samples (m = 1,2,3,…., *M*), $T_s = \Delta_k = t_k - t_{\kappa\text{-}1}$ is the inter sample interval then the backward difference of fractional order function is given as:

$$\Delta_k^{\alpha} f(t_k) = \sum_{m=0}^{(t_M - t_0)/\Delta_k} c_m^{\alpha} f(t_k - mk)$$

Where c_m are the consecutive coefficients which are basically the binomial coefficients.The basis function $f(t_k)$ is defined as:

$$f(t_k) = \log(1 + e^{\beta t_k})$$

Where β is the inclination coefficient.

The output of FO-ANN-CLPC-ACP1000 is given as:

$$\hat{Y}_{n_r}(t_k) = \Delta_k^{\alpha} f\left[\sum_{n_q=1}^{q} w_{nq,nr}^{i} \Delta_k^{\alpha} f\left(\sum_{n_p=1}^{p} w_{np,nq} u_{n_p}^{i}(k)\right)\right]$$

The performance index of FO-ANN-CLPC-ACP1000 is given as:

$$J = \frac{1}{2}\sum_{n_r,j}\left[y_j(k) - \hat{y}_{n_r}(t_k)\right]^2$$

Now, the weights updating logic for output layer is computed as:

$$\Delta w_{n_q,n_r}^{i}(k) = \eta\theta_{I_{n_q}}^{i}\left[y_j(k) - \theta_{H_{n_r}}^{i}\right]\frac{\partial\theta_{H_{n_r}}^{i}(k)}{\partial e_{H_{n_r}}^{i}}$$

Where η is the learning rate.

Now, the weights updating logic for the hidden layer is computed as:

$$\Delta w_{n_p,n_q}^{i}(k) = \eta u_{I_{n_p}}^{i}\sum_{n_r} w_{n_q,n_r}^{i}\frac{\partial\theta_I^{i}}{\partial e_{I_{nq}}^{i}}\left[y_j(k) - \theta_{H_{n_r}}^{i}\right]\frac{\partial\theta_{H_{n_r}}^{i}(k)}{\partial e_{H_{n_r}}^{i}}$$

The accuracy of the FO-ANN-CLPC-ACP1000 is measured in terms of goodness of fit (FIT), which is computed as:

$$FIT_j = \left(1 - \frac{\|y_j - \hat{y}_j\|}{\|y_j - \bar{y}_j\|}\right)\times 100\%$$

Where y_j is the *j*-th actual output of CCLD-MIMO model of ACP1000, is the j-th predicted output of FO-ANN-CLPC-ACP1000 and $\bar{y}_j$ is j-th mean of the actual output of CCLD-MIMO model of ACP1000.

3. RESULTS AND DISCUSSION

The closed loop training and testing framework of primary circuit of ACP1000 is shown in Figure 4. A state-of-the-art novel virtual Instrument (VI) is designed for FO-ANN-CLPC in LabVIEW, as shown in Figure 5.

The block diagram of FO-ANN-CLPC VI configured in training phase is shown in Figure 6.

3.1 Performance Evaluation of FO-ANN-CLPC in LabVIEW

In this research work, the testing of the FO-ANN-CLPC tool is performed in LabVIEW. In closed loop training and testing framework of the primary circuit of ACP1000, reactor power transient data with a data set of 60% samples and 40% samples are selected for reactor shutdown, power-up, power-down and steady power operational data, respectively. In the testing phase, the predicted normalized reactor power which is an ANN approximation tested against the cluster of normalized reactor power. A sample testing part is shown in Figure 7 against a few samples of the real cluster of reactor power data.

In validation phase, the comparison of measured and predicted reactor power is shown in Figure 8.

The error between the measured and predicted reactor power is shown in Figure 9. The predicted reactor power follows the measured reactor power with minimizing error function in transient condition. In order to assess the accuracy of the minimizing error, the zoomed view of the error is shown in Figure 10.

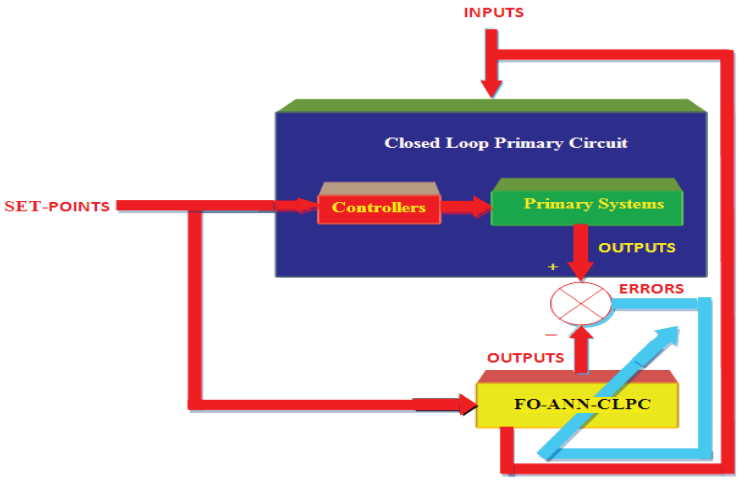

Fig. 4. Closed loop framework for FO-ANN-CLPC design of ACP1000.

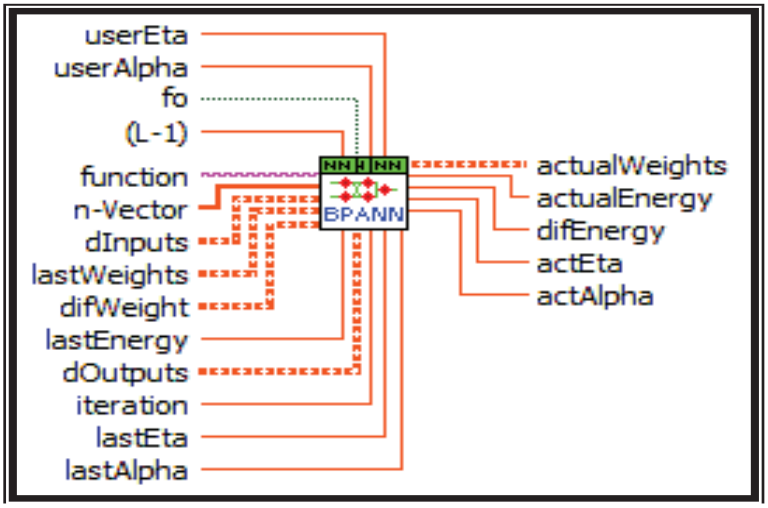

Fig. 5. Fractional order BP neural network VI.

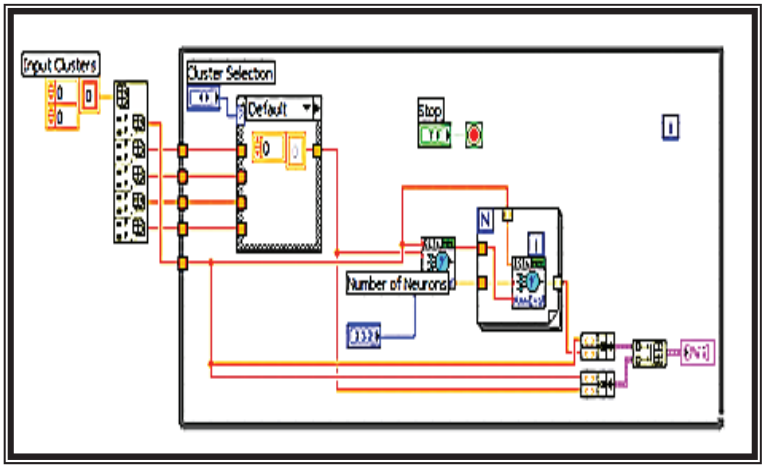

Fig. 6. Fractional order BP neural network training VI.

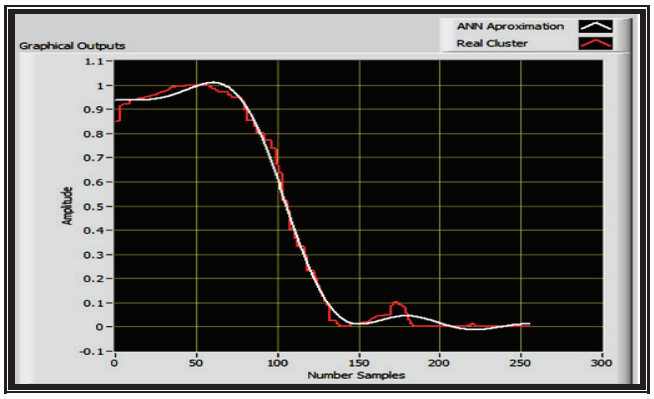

Fig. 7. Comparison of ANN and normalized real reactor power front panel in testing phase.

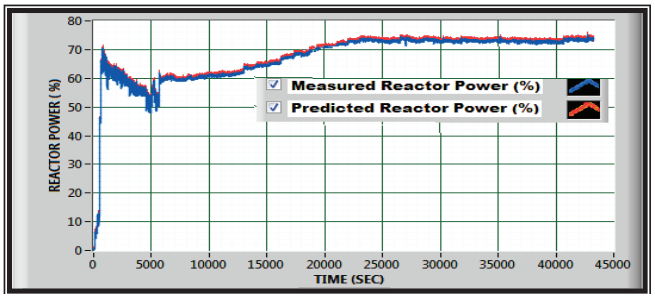

Fig. 8. Comparison of measured and predicted reactor power in validation phase.

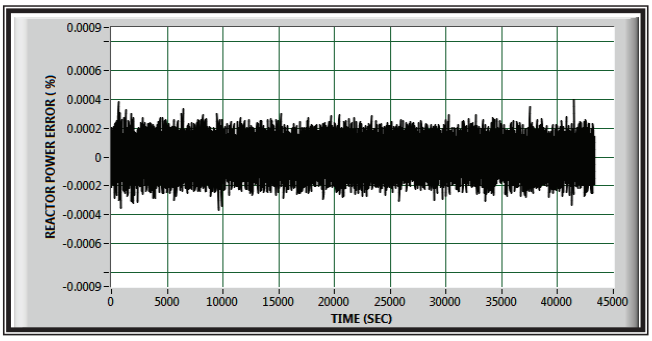

Fig. 9. Error between measured and predicted reactor power.

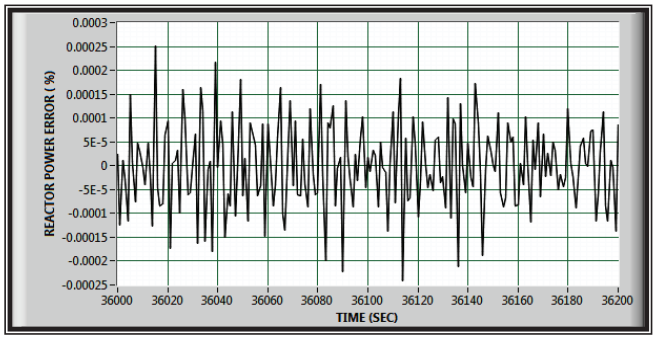

Fig. 10. Zoomed view of error between measured and predicted reactor power.

The parameters of FO-ANN-CLPC-ACP1000 are tabulated in Table 1. The computational performance of FO ANN is gauged in simulations in terms of goodness of fit (FIT).

Table 1. Parameters of FO-ANN-CLPC-ACP1000 model

CCLD-MIMO Model Parameters	Design Values
p- q- r Topology	6-40-6
Sampling Time (T_s), Sec	0.1
Number of training patterns (M)	43,5000
Fractional Order (α)	0.9575
Inclination Coefficient (β)	1
Learning Rate (η)	0.65
FIT_1	94.86%
FIT_2	96.55%
FIT_3	95.37%
FIT_4	95.88%
FIT_5	96.12%
FIT_6	95.98%

3.2. Transient Dynamic Simulation of FO-ANN-CLPC in LabVIEW

Now, in this research work, the performance of FO-ANN-CLPC-ACP1000 is evaluated in transient simulation experiments. In this dynamic study, the turbine load which is also known as power turbine load expressed in % is increased from 20% to 100% as per procedure as laid down in [1,3] and various parameters are simulated and analyzed against this transient power turbine load in LabVIEW environment. For the sake of better understanding and inter comparison purposes, all power dependent parameters are plotted on same time scale. Similarly, other thermal parameters, pressure hydraulic parameters, level hydraulic parameters and flow hydraulic parameters are plotted on same time scales.

The turbine power or power turbine load and power reactor power or power neutron flux are both dependent parameters and their dynamic behavior is shown in Figure 11.

Figure 11 clearly proves that power neutron flux follows the power turbine load. This plot also proves the overall performance of closed loop dynamics. The power neutron flux drops initially because of inverse Xenon dynamics as the power turbine load demands the increasing power signal which is compensated by the lead compensator when the turbine power stabilizes around 30%. When turbine power takes up the next sequence of ramp-up for power rising transient then leading dynamics of reactor power controller appears and a slight little over shoot is observed in the dynamic behavior.

The dynamic simulation of thermal parameters is shown in Figure 12.

The pressurizer saturation temperature remains around 345 ^{O}C. Hot leg temperature increases as the reactor power increases but the cold leg temperature decreases because of the gain in hot leg temperature and pressurizer controls provided on the hot leg. Reactor coolant average temperature follows the averaging dynamics of cold and hot leg temperatures.

The dynamic simulation of thermal parameters

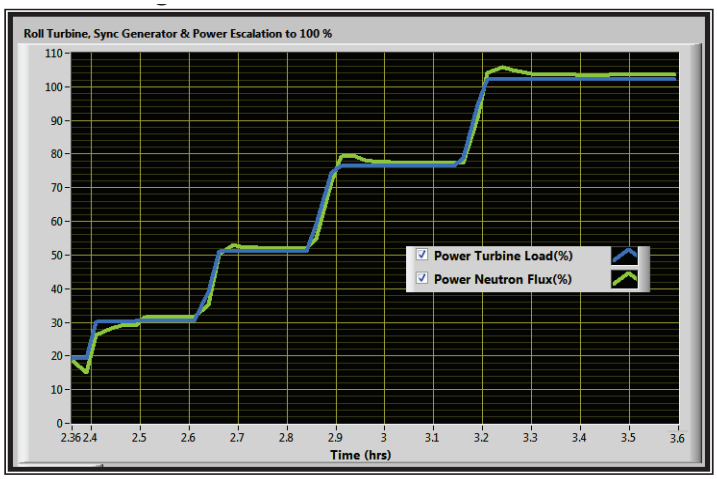

Fig. 11. Dynamic simulation of reactor power and turbine power.

is shown in Figure 13.

The pressurizer saturation temperature remains around 345 ^{0}C. Hot leg temperature increases as the reactor power increases but the cold leg temperatures decreases because of the gain in hot leg temperature and pressurizer controls provided on the hot leg. Reactor coolant average temperature follows the averaging dynamics of cold and hot leg temperatures.

The dynamic simulation of pressure hydraulic parameters is shown in Figure 14. The reactor coolant pressure is kept constant by pressurizer pressure controller. The steam pressure decreases as the turbine load increases that proves the inverse relationship between the turbine power and steam pressure.

The dynamic simulation of level hydraulic parameters is shown in Figure 15.

The steam generator level decreases due to the increase in turbine power and decrease in steam pressure. Since the reactor coolant pressure and pressurizer saturation temperatures are almost constant, therefore, the pressurizer level controller increases the pressurizer level as the reactor power and reactor coolant average temperature increases. The dynamic simulation of flow hydraulic parameters is shown in Figure 16.

Figure 17 also clearly proves that feed water flow follows the steam generator flow. This plot also proves the overall performance of closed loop dynamics. When steam generator flow increases due to the increase in turbine power then the leading dynamics feed water flow appears and a slight little over shoot is observed in the dynamic behavior on every increase in turbine power ramp-up transient.

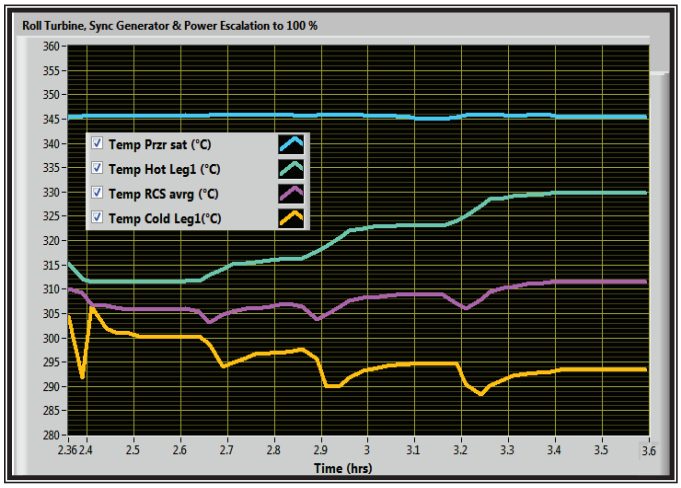

Fig. 13. Dynamic simulation of thermal parameters

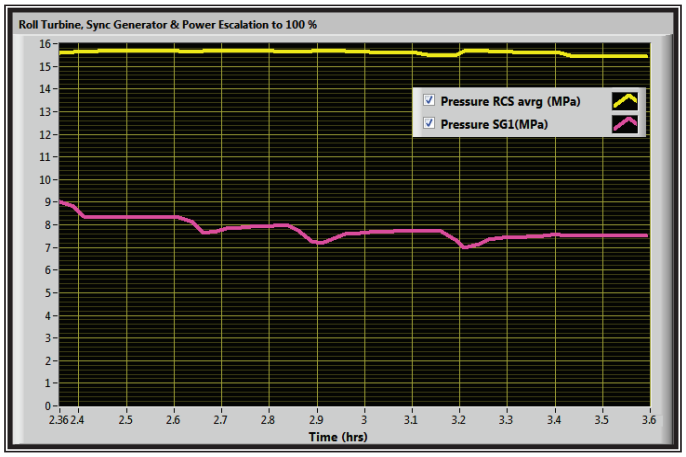

Fig. 14. Dynamic simulation of pressure hydraulic parameters.

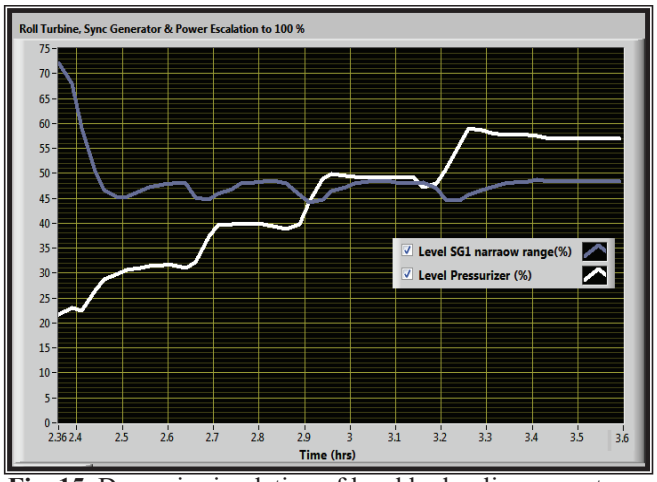

Fig. 15. Dynamic simulation of level hydraulic parameters

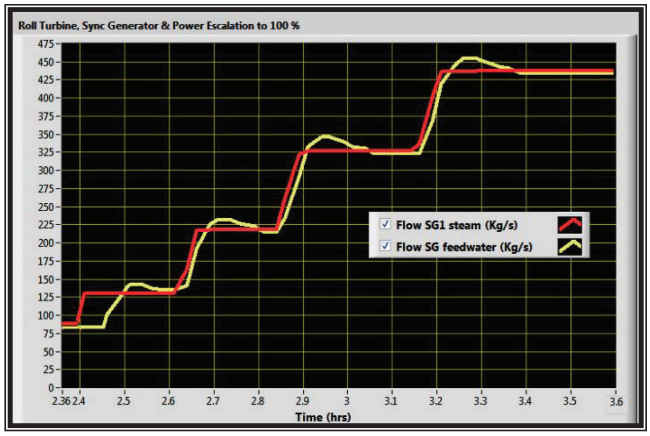

Fig. 17. Dynamic simulation of flow hydraulic parameters.

4. CONCLUSION

The dynamics of the primary circuit of a third generation ACP1000 nuclear power plant has been focused on in this research work. The coupled nonlinear dynamics of reactor power control system (G-bank), reactor power control system (R-bank), pressurizer pressure control system, pressurizer level control system, digital electro-hydraulic control system, steam generator water level control system and steam dump control system has been identified in MIMO framework. Parameters of closed loop MIMO system are estimated by a new specialized tool developed for the first time in LabVIEW. The new specialized tool is a mathematical fractional order differential equations based on graphical code. The evaluation of the designed tool is proved successful and upto mark through dynamic transient simulation experiments of reactor power following turbine power. The proposed model and tool can be extended for secondary circuit and accident analysis in future.

5. ACKNOWLEDGMENT

The support of the Pakistan Atomic Energy Commission, Chashma Centre of Nuclear Training and Computer Development Division of KANUPP is gratefully acknowledged.

6. CONFLICT OF INTEREST

The authors declare no potential conflict of interests.

7. REFERENCES

1. Preliminary safety report of HPR1000. UKHPR1000GDA Project, Report HPR/GDA/PSR: (2017).
2. T. Xin. Safety approach and safety assessment Hualong HPR1000, IFNEC Report: (2018).
3. L. C. C. Po, and J. M. Link. PCTRAN-3 / U 3-LP.

Micro-Simulation Technology: (2018).

4. N. Zare, G. Jahanfarnia, A. Khorshidi, and J. Soltani. Robustness of optimized FPID controller against uncertainty and disturbance by fractional nonlinear model for research reactor. *Nuclear Engineering and Technology* 52: 2017-2024 (2020).
5. M. Pakdaman, A. Ahmadian, S. Effati, S. Salahshour, and D. Baleanu. Solving differential equations of fractional order using an optimization technique based on training artificial neural network. *Applied Mathematics and Computations* 293: 81-95 (2017).
6. W. Wang, and Y. Qiao. Dynamic analysis of fractional-order recurrent neural network with caputo derivative. *International Journal of Bifurcation and Chaos* 27 (02): 01-13 (2017).
7. M. A. Jamal, F. Hanif, M. S. A. Khan, and S. Inayatullah. Neural minimization methods (NMM) for solving variable order fractional delay differential equations (FDDEs) with simulated annealing (SA). *PLoS ONE* 14 (10): 1-22 (2019).
8. M. R. Rahmani, and M. Farrokhi. Nonlinear dynamic system identification using neuro-fractional order Hammerstein model. *Transactions of the Institute of Measurements and Control*: 01-12 (2017).
9. W. Cheng, A. Wu, J. Zhang, and B. Li. Outer synchronization of fractional-order neural networks with deviating argument via centralized and decentralized data-sampling approaches. *Advances in Difference Equations*: 01-31 (2019).
10. X. Zhang, and C. Yang. Neural network synchronization of fractional-order chaotic systems subject to backlash nonlinearity. *AIP Advances* 10: 01-08 (2020).
11. H. Jahanbakhti. A novel fractional-order neural network for model reduction of large scale systems with fractional-order nonlinear structure. *Soft Computing*: 01-11 (2020).
12. G. Nassajian, and S. Balochian. Multi-model estimation using neural network and fault detection in unknown time continuous fractional order nonlinear systems. *Transactions of the Institute of Measurements and Control*: 01-13 (2020).
13. J. Wu, P. Chen, C. Li, Y. Kuo, N. Pai, and C. Lin. Multilayer fractional order machine vision classifier for rapid typical lung diseases screening on digital chest X-ray images. *IEEE Access* 08: 01-17 (2020).
14. Wan, X. Jhan, H. Gao, Q. Yang, T. Han, and M. Ye. Multiple asymptotical stability analysis for fractional-order neural networks with time delays. *International Journal of Systems Science*: 01-14 (2019).
15. Y. Zhao, X. Du, and G. Xia. A novel fractional-order PID controller for integrated pressurized water reactor based on wavelet kernel neural network algorithm. *Mathematical Problems in Engineering* : 01-13 (2014).
16. J. Wan, P. Wang, and F. Zhao. Decoupling control of both turbine power and reactor power in a multi-reactor and multi-turbine nuclear power plant. *Progress in Nuclear Energy* 132: 01-16 (2021).